electronics

MDPI

Article

Printed Closely Spaced Antennas Loaded by Linear Stubs in a MIMO Style for Portable Wireless Electronic Devices

Aqeel Ahmed Khan [1], Muhammad Saeed Khan [2], Syed Aftab Naqvi [3], Bilal Ijaz [3], Muhammad Asif [4,*], Esraa Mousa Ali [5], Salahuddin Khan [6], Ali Lalbakhsh [7], Mohammad Alibakhshikenari [8,*] and Ernesto Limiti [9]

1 Department of Electrical Engineering, Faculty of Engineering and Applied Sciences, Riphah International University, Islamabad 44000, Pakistan; aakj666@gmail.com
2 Department of Information Engineering, University of Padova, Via Gradenigo 6/b, 35131 Padova, Italy; mskj786@hotmail.com
3 Department of Electrical and Computer Engineering, COMSATS University Islamabad, Islamabad 45550, Pakistan; aftabnaqvi@cuisahiwal.edu.pk (S.A.N.); bilal_ijaz@comsats.edu.pk (B.I.)
4 Department of Electrical Engineering, University of Science & Technology, Main Campus, Township Bannu, Bannu 28100, Pakistan
5 Faculty of Aviation Sciences, Amman Arab University, Amman 11953, Jordan; esraa_ali@aau.edu.jo
6 Electrical Engineering Department, College of Engineering, King Saud University, Riyadh 11421, Saudi Arabia; khanheu@gmail.com
7 School of Engineering, Macquarie University, Sydney, NSW 2109, Australia; ali.lalbakhsh@mq.edu.au
8 Department of Signal Theory and Communications, Universidad Carlos III de Madrid, 28911 Leganés, Madrid, Spain
9 Electronic Engineering Department, University of Rome "Tor Vergata", Via Del Politecnico 1, 00133 Rome, Italy; limiti@ing.uniroma2.it
* Correspondence: masifeed@ustb.edu.pk (M.A.); mohammad.alibakhshikenari@uc3m.es (M.A.)

Abstract: An easy-to-manufacture and efficient four-port-printed Multiple Input Multiple Output (MIMO) antenna operating across an ultra-wideband (UWB) region (2.9–13.6 GHz) is proposed and investigated here. The phenomenon of the polarization diversity is used to improve the isolation between MIMO antenna elements by deploying four orthogonal antenna elements. The proposed printed antenna ($40 \times 40 \times 1.524$ mm^3) is made compact by optimizing the circular-shaped radiating components via vertical stubs on top of the initial design to maximally reduce unwanted interaction while placing them together in proximity. The measurements of the prototype MIMO antennas corroborate the simulation performance. The findings are compared to the recent relevant works presented in the literature to show that the proposed antenna is suitable for UWB MIMO applications. The proposed printed UWB MIMO antenna could be a good fit for compact portable wireless electronic devices.

Keywords: printed MIMO antennas; orthogonal radiating elements; polarization diversity; ultra-wideband; linear stubs; portable wireless electronic devices

Citation: Khan, A.A.; Saeed Khan, M.; Naqvi, S.A.; Ijaz, B.; Asif, M.; Ali, E.M.; Khan, S.; Lalbakhsh, A.; Alibakhshikenari, M.; Limiti, E. Printed Closely Spaced Antennas Loaded by Linear Stubs in a MIMO Style for Portable Wireless Electronic Devices. *Electronics* **2021**, *10*, 2848. https://doi.org/10.3390/electronics10222848

Academic Editors: Adão Silva, Daniel Castanheira and Rui Dinis

Received: 29 October 2021
Accepted: 16 November 2021
Published: 19 November 2021

1. Introduction

The Federal Communication Commission (FCC) permitted the use of the ultra-wideband (UWB) spectrum ranging from 3.1 GHz to 10.6 GHz for commercial applications [1–3]. Low data transmission due to limited power spectral density and multipath fading in dense propagation environments restricted the UWB to indoor applications only. The suitable solution for the UWB was to integrate with the MIMO systems, improving spatial-multiplexing gain and array gain, which consequently enhances the spectral performance [4–6]. Moreover, the data rate of the UWB-MIMO system is significantly increased because the channel capacity of the UWB system is proportional to the number of antennas [7]. Thenceforth, researchers turned their efforts to developing MIMO systems for the electronic devices operating in the UWB region in order to alleviate the power limit congestion [8–24].

Although UWB provides a wide range of diversity in time domain and bandwidth, the unprecedented growth in complex wireless systems, internet-connected devices, and IoT models necessitates a larger amount of bandwidth. The International Telecommunication Union (ITU) has proposed the 11 GHz (10.7 to 11.7 GHz) and 13 GHz (12.75 to 13.25 GHz) frequency bands for wireless networks in response to the need for more bandwidth [25,26]. There are already several works reported to utilize this extended W-UWB region [21,22].

A planar UWB-MIMO antenna with a 7.5 GHz bandwidth for high isolation is proposed in [8], but the antenna size is incompatible with lightweight portable devices. A large size antenna with four elements based on a neutralization technique is presented in [9] to obtain very low coupling (23 dB), but the proposed technique reduced the efficiency of the design as well. Another large size antenna (4000 mm^2) with improved efficiency but reduced bandwidth is proposed in [10]. A comparable design in terms of size is proposed in [11], but the methodology deployed to build the design and resultantly minimize the self-coupling is very complex. Moreover, a higher bandwidth of 8 GHz is achieved with a trade-off of 75% efficiency. In [12], I-shaped grounded stubs are placed to achieve high isolation for a semi-circular shape MIMO antenna operating from 1.9 to 10.2 GHz, whereas the size of the reported antenna is 1750 mm^2, which is, in comparison, on the larger side. Another large diversity antenna with a mushroom and electronic band gap (EBG) structure is proposed in [13]. Non-planar (three-dimesional) antennas with four and eight elements are proposed in [14–16]. These designs exploit polarization diversity and due to angular placement, complexity and being difficult to produce, they are unsuitable for planar structures. In [17], a fractal-octagonal shape was used to achieve a wideband of 8.6 GHz with less than 17 dB mutual coupling between components, and the covered band ranged from 2 to 10.6 GHz. In [18], a reconfigurable geometry for designing an MIMO antenna, with self-coupling between elements around 20 dB and wideband spanning from 2 to 11 GHz, is proposed. A split-ring resonator (SSR) antenna with four elements is also proposed in [19]. The obtained bandwidth is only 4.08 GHz (2.2 to 6.28 GHz) with 65% efficiency and 2025 mm^2 board size. A compact and polarization diversity antenna with four elements is also proposed in [20] to operate in a slightly wider band (3.1 to 11 GHz) than UWB. Again, complex geometry is used to obtain a larger bandwidth of 9 GHz (3 to 12 GHz), but gain is compromised [21]. Although the designs reported in [23,24] utilized simple but different structures in orthogonal planes, the overall size becomes 2500 mm^2.

Recently, authors have presented a miniaturized four-port antenna for UWB, 11 and 13 GHz frequency bands with an overall attained bandwidth of 10.5 GHz (3 to 13.5 GHz); however, the mutual coupling was around −15 dB, ECC was around 0.4 and CLL was 0.22 bits/s/Hz [26]. The proposed design was initiated using the same patch and later modified to obtain the desired results of −16 dB mutual coupling and 90% efficiency over the wider bandwidth without compromising the overall physical size of the antenna. The larger size of the radiating patch of a unit cell in [26] causes greater current flow and unwanted interaction between the adjacent elements of the proposed MIMO antenna. This consequently increases the mutual coupling and efficiency of the MIMO antenna. Moreover, with the excess current on the edges of the square patch, the MIMO antenna could cause electromagnetic interference with the rest of the integrated RF circuitry in an electronic device. This could affect the overall efficiency of the device. So, the reciprocal of the square patch attached on the edge of the circular patch to enhance the bandwidth is required, but carefully, as it deals with the enhancement of the bandwidth of the proposed MIMO antenna in [26].

Although the research and literature to design a UWB-MIMO antenna is progressive, the need to design a relevantly efficient and broadband MIMO antenna, which is also easy to design, is present. All the above-mentioned designs have compromises between board size, bandwidth, efficiency performance, design complexity, and the number of ports to be accrued within a limited size. MIMO antennas presented in [9,11,12,17,18] have the smallest dimensions; however, some of these lightweight architectures have difficult-to-implement and complex decoupling mechanisms, while others have lower bandwidth and

efficiencies. Compared to these current designs, the proposed design is compact, highly efficient and covers a larger bandwidth. As a result, the proposed work aims to design a simple and miniaturized four-element antenna with a broad bandwidth and high efficiency.

A compact and easy-to-integrate W-UWB MIMO antenna with a bandwidth of 10.7 GHz ranging from 2.9 to 13.6 GHz is discussed in this paper. The proposed frequency band includes the UWB allocated by the FCC, 11 GHz and 13 GHz frequency bands recommended by the ITU for the commercial wireless electronic applications, so it is named as W-UWB. The paper is organized as follows: the design of the unit cell is presented in Section 2, while design and parameters of the MIMO antenna are discussed in Section 3. The conclusion of the work is presented in Section 4.

2. Design of the Unit Cell for The MIMO Antenna

Figure 1 shows a diagram of the unit cell for the orthogonal MIMO antenna. Initially, a circular patch with a radius of 5 mm attached to a 10.1 mm-long feed line was etched on a partly ground (6.25 × 13.5 mm^2) TMM4 laminate with a thickness of 1.524 mm, $\varepsilon r = 4.4$ and $\tan \delta = 0.02$. The simulations were carried out in Ansys High-Frequency Structure Simulator (HFSS). A wideband impedance match from 3.8 GHz to 12.6 was obtained as depicted in Figure 2. If the radius of the circular patch is increased, a good impedance match at the lower band could be achieved, but this could affect the coupling in the MIMO configuration. To achieve a wider bandwidth, the top side of the circular patch was modified with vertical stubs of dimensions 2.45 × 0.5 mm^2. The optimized vertical stubs caused an increased current density on the surface of the overall radiating patch. Consequently, the matched impedance bandwidth increased on both the lower and higher sides of the earlier achieved band, and thus a UWB of 10.7 GHz from 2.9 to 13.6 GHz was achieved.

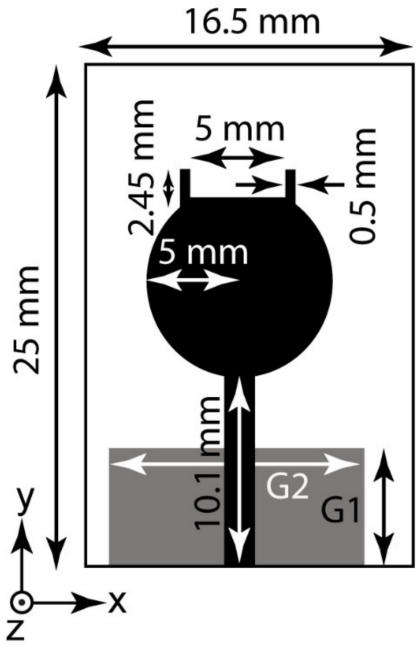

Figure 1. Diagram of the stub-loaded circular MIMO antenna.

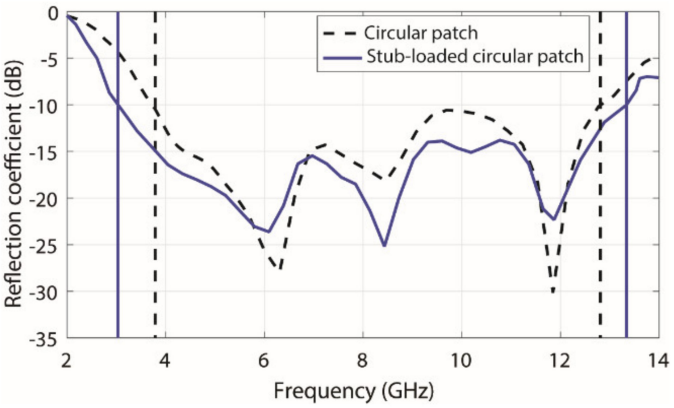

Figure 2. S_{11} of circular patch and stub-loaded circular patch.

Figure 2 shows a comparison of the reflection coefficients (S11) of circular and stub-loaded circular patches. To highlight the extension in bandwidth by addition and optimization of the vertical stubs, the lower and upper operating frequencies for circular and modified stub-loaded patches are shown by the vertical dotted line and solid line, respectively).

In addition to other antenna parameters, a fragmentary ground plane was introduced beneath the transmission line to alter and reconfigure the surface current density. The inclusion of this partial ground plane affected the impedance matching and consequently the S-parameters. It is observed that the overall bandwidth of the reflection coefficient reduced when the width of the ground (G1) is decreased or increased from 6.25 mm. As shown in Figure 3a, decreasing G1 affects the lower frequency band while increasing G1 affects the high frequency band. On the other hand, the length of the ground (G2) has no impact on the unit cell's total bandwidth. However, as shown in Figure 3b, it influences the magnitude of the matched impedance. Based on these findings, the partial ground was optimized as 6.25×13.5 mm^2 to better accommodate the UWB.

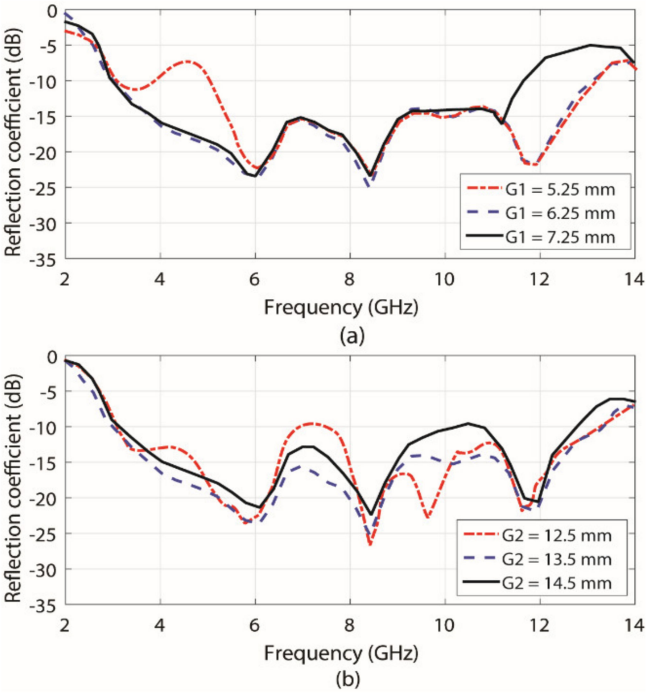

Figure 3. The parametric study of ground plane (**a**) width effects, (**b**) length effects.

3. Design of the Four-Port MIMO Antenna

The four-port MIMO antenna was then designed by using the unit cell presented in Section 2. Four cells in close vicinity were mounted using reciprocal orthogonal geometry, as shown in Figure 4. The distance between two radiating patches was kept at 5.25 mm. Figure 5a,b illustrate the antenna prototype, while Figure 5c illustrates the experimental setup to measure different antenna parameters. The prototype was etched on 1.524 mm-thick TMM4 laminate (εr = 4.4 and tan δ = 0.02) using a LPKF ProtoMat S64 machine and SMA connectors were soldered to measure the antenna performance.

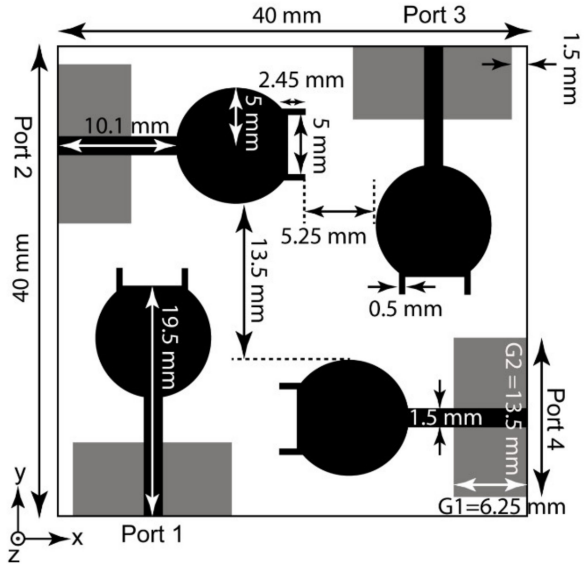

Figure 4. Schematic of the proposed UWB MIMO antenna.

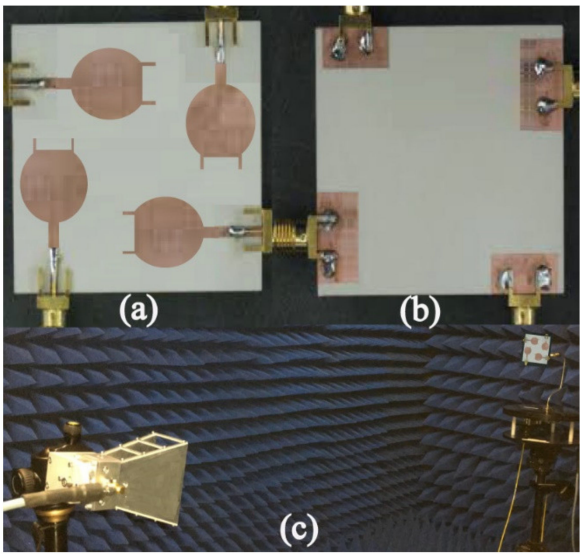

Figure 5. Snapshot of the proposed UWB MIMO antenna. (**a**) Radiating Patch side, (**b**) Partial Ground side, (**c**) Measurement Setup.

3.1. S-Parameters

The simulated and measured S-parameters of the MIMO antenna are shown and compared in Figure 6. Figure 6a depicts the measured reflection coefficients at all four ports and simulated S_{11} for port 1 only. The rest of the simulated parameters are like S_{11}, so are not shown in pictorial view for the sake of clarity. Although a slight shift in simulated

and measured S_{11} at lower frequencies is observed, it remains below −10 dB throughout the proposed wideband.

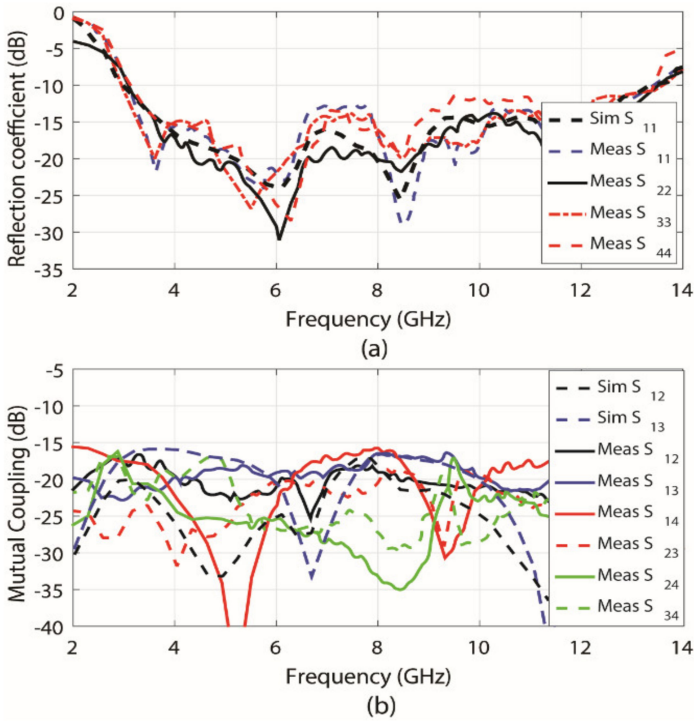

Figure 6. Simulated and measured S-parameters of the 4 ports (**a**) reflection (**b**) mutual coupling.

Figure 6b depicts and compares the mutual coupling between any two ports. It is observed that the simulated and measured mutual coupling at the respective port is less than −16 dB, indicating that the elements are isolated even when they are close together. Furthermore, the EM coupling between crossed element couples such as 2, 4 and 1, 3 is less than −16 dB. Next, the effects of the connected ground were observed; as is the case with most of the MIMO designs, all the partial grounds were connected through a 0.5 mm-thick TL. However, negligible effects were recorded on the discussed results. That is why all the measurements were carried out on the design depicted in Figure 4.

3.2. Surface Current Density

The current density of an antenna is an important parameter for demonstrating polarization diversity phenomena. To demonstrate it, one port at a time was excited and the rest of the ports were terminated with the matched load; current density at 5.5 GHz is shown in Figure 7. Figure 7a shows that y-directed linearly polarized current vector lines reside around the TL and edges of the circular patch if port 3 is excited. However, when port 2 is excited, x-directed linearly polarized current vector lines with equal magnitude around the same geometry corners are observed. This clearly indicates polarization diversity among the elements of the MIMO antenna. The excellent separation between the elements in proximity is due to these orthogonally polarized current vectors.

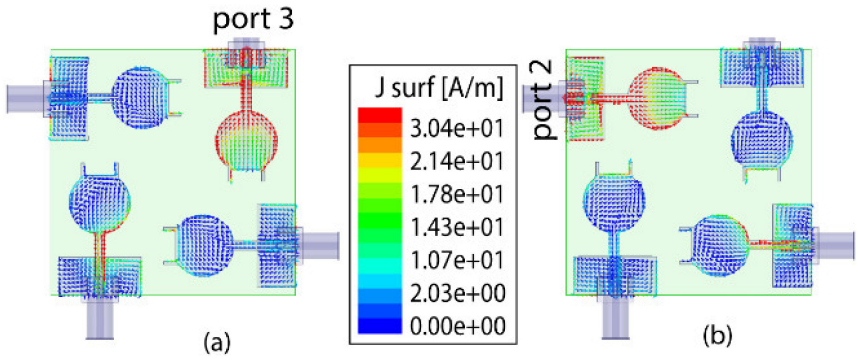

Figure 7. Screenshots of the current density at surface of the antenna operating at 5.5 GHz while excited ports are (**a**) 3, (**b**) 2.

3.3. Radiation Pattern in Different Planes at Different Frequencies

Figure 8 describes and compares the simulated and measured results of the far-field radiation patterns and gains in the x–z and y–z planes at 4, 7.5 and 10.5 GHz when either port 1 or port 2 of the MIMO antenna is excited.

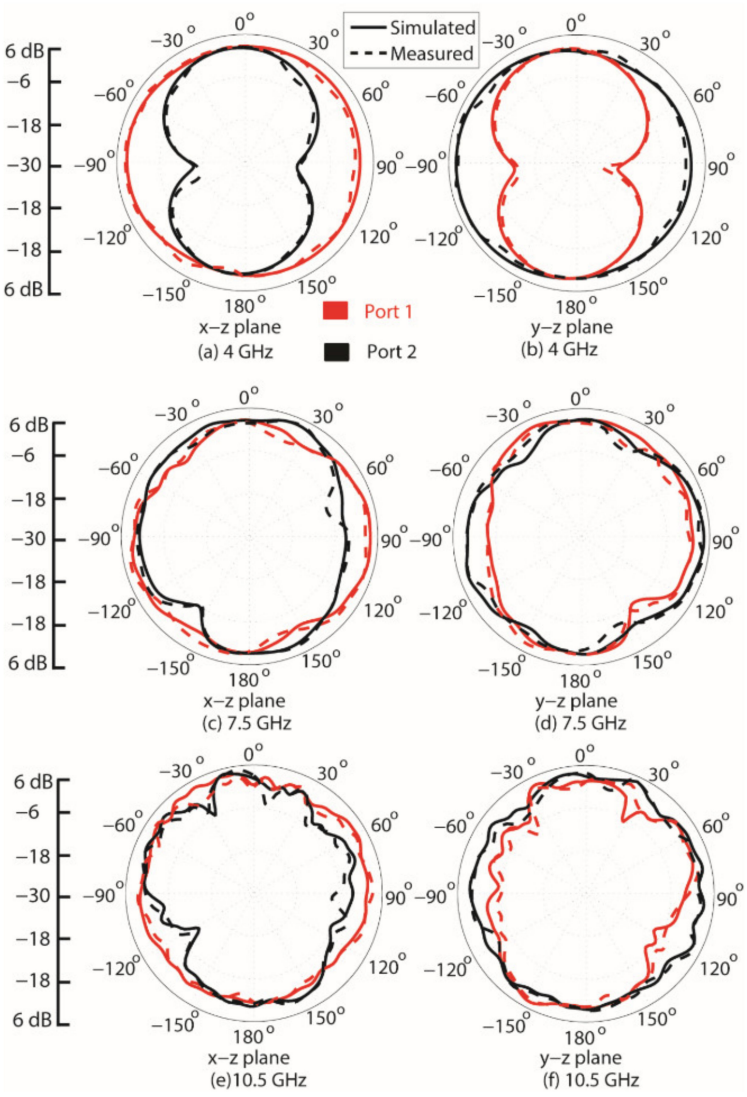

Figure 8. 2D Radiation patterns in X–Z and Y–Z planes at 4.0 GHz, 7.5 GHz, and 10.5 GHz.

Figure 8a shows an omni-directional radiation pattern in the x–z plane at 4 GHz when port 1 is excited, whereas a dumbbell-shaped radiation pattern is observed in the same plane at the same frequency when port 2 is excited. The results are exactly inverted in the y–z plane for the two ports as shown in Figure 8b. Here, in Figure 8b, in the y–z plane, when port 1 is excited, the antenna exhibits a dumbbell-shaped pattern instead of an omni-directional one, as was the case in Figure 8a. Furthermore, port 2 shows an omni-directional shape instead of a dumbbell shape. This is quite expected in the case of MIMO antennas when polarization diversity is deployed to increase the isolation at different ports. It confirms that the elements have orthogonal polarization, and that the polarization diversity is employed between two closely spaced elements. It can be observed that the measured results are well matched with the simulated results and small deviations are due to fabrication tolerance.

To validate this fact, radiation patterns of ports 1 and 2 were analyzed in the x–z and y–z planes at different frequencies. Figure 8c shows the radiation pattern of the two ports in the x–z plane at 7.5 GHz, whilst Figure 8d shows this pattern in the y–z plane at the same frequency. However, the patterns are not of a uniform shape like at 4 GHz in Figure 8a,b, i.e., omni-directional or dumbbell shaped. The reversal of the pattern in different planes is observed clearly. The pattern of port 1 in the x–z plane is the pattern of port 2 in the y–z plane, and vice versa at 7.5 GHz as well, which strengthens the phenomenon of polarization diversity. Moreover, the radiation patterns of ports 1 and2 at 10.5 GHz, the maximum frequency attained, in the x–z and y–z planes were also analyzed in Figure 8e,f. It is reported that the patterns of a port in the respective plane is an exact inversion of the patterns of the other port in the same plane at 10.5 GHz. At higher frequencies, discrepancy in the measured results is slightly more than the simulated results due to fabrication tolerance, connector losses, soldering and cable losses.

Next, to foster the discussion, a 3D radiation pattern at 3.5 GHz is plotted in Figure 9. It is observed that, when port 3 is excited, then the nulls and maximums of the resultant radiation pattern are exactly orthogonal to the nulls and maximums when port 2 is excited, as shown in Figure 9a,b. At the points where port 3 has the minimum points, port 2 has the maximum points and vice versa, so the resultant patterns are completely uncorrelated. Hence, the phenomenon of polarization diversity is validated through 2D and 3D radiation patterns at different frequencies.

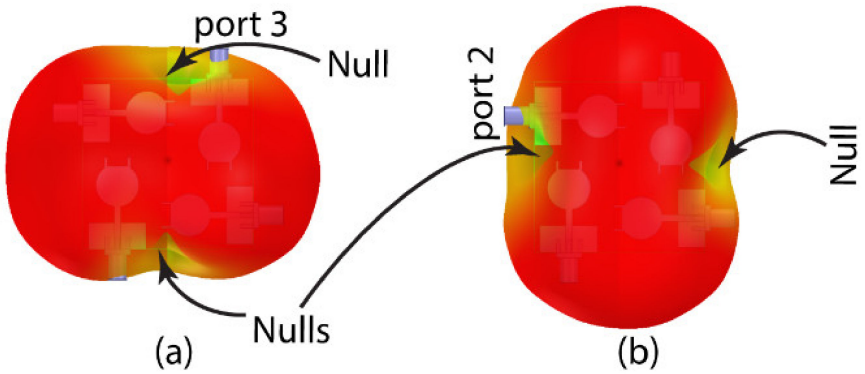

Figure 9. 3D radiation patterns at 3.5 GHz while exciting port (**a**) 3 only, (**b**) port 2 only.

Furthermore, peak gain and efficiency of the antenna for the entire frequency band is reflected in Figure 10. The average gain of 4.5 dBi with more than 90% efficiency is reported for the entire spectrum to confirm the antenna functionality in the UWB region.

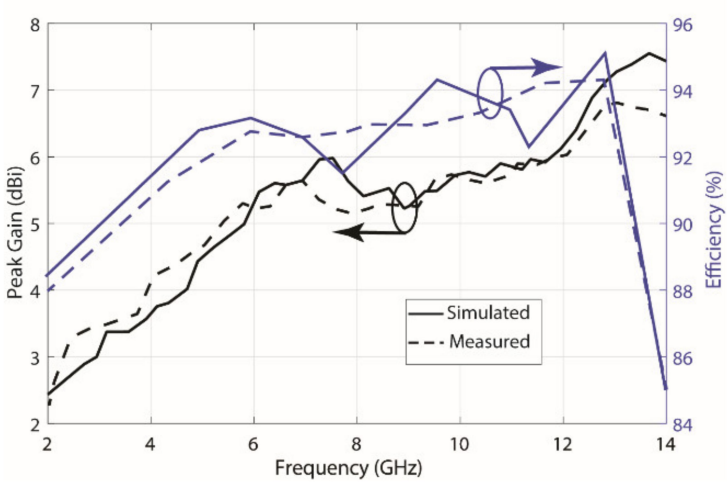

Figure 10. Peak Gain and efficiency of the MIMO antenna.

3.4. Diversity Analysis

Envelope Correlation Coefficient (ECC) is a useful metric for assessing the diversity of the MIMO antenna components. High diversity and low ECC are the consequences of low coupling and different radiation patterns in a single plane. Equation (1) [27] was used to calculate the ECC of the proposed MIMO antenna by using far-field radiation plots.

$$\rho_e = \frac{\left|\int_0^{2\pi}\int_0^{\pi}\left(XPR{\cdot}E_{\theta1}{\cdot}E_{\theta2}^{*}{\cdot}P_{\theta}+E_{\varphi1}{\cdot}E_{\varphi2}^{*}{\cdot}P_{\varphi}\right)d\Omega\right|^2}{\int_0^{2\pi}\int_0^{\pi}\left(XPR{\cdot}E_{\theta1}{\cdot}E_{\theta1}^{*}{\cdot}P_{\theta}+E_{\varphi1}{\cdot}E_{\varphi1}^{*}{\cdot}P_{\varphi}\right)d\Omega\times\int_0^{2\pi}\int_0^{\pi}\left(XPR{\cdot}E_{\theta2}{\cdot}E_{\theta2}^{*}{\cdot}P_{\theta}+E_{\varphi2}{\cdot}E_{\varphi2}^{*}{\cdot}P_{\varphi}\right)d\Omega} \quad (1)$$

In the expression above, XPR stands for the cross-polarization ratio, while$\cdot P_\theta$ and P_φ are θ and φ components of the angular density functions of an excited wave. Figure 11a depicts the calculated ECC values for the entire frequency spectrum for isotropic, indoor, and outdoor Gaussian. The far-field characteristics in a uniform scattering environment were utilized to calculate the isotropic case, whereas the far-field radiation characteristics in a complex environment were used for the indoor and outdoor Gaussian. The fact that the computed ECC values for the isotropic case are less than 0.13, while the values for the indoor and outdoor Gaussian are less than 0.26 and 0.38, respectively, demonstrates the antenna polarization diversity once again.

Channel Capacity Loss (CCL) is another way to measure the importance of a MIMO antenna. The CCL of ports 1 and 2 and 3 and 4 versus frequency is shown in Figure 11b. The overall computed CCL between the respective ports is less than 0.21 bits/s/Hz, indicating that there is a very little interaction between any two adjacent ports. Furthermore, Figure 12 shows the diversity gain and multiplexing efficiency across the entire spectrum, demonstrating the diverse MIMO antenna functionality. Throughout the claimed frequency range, the diversity gain is stated to be about 10 dB, while the multiplexing efficiency is greater than −3.5 dB.

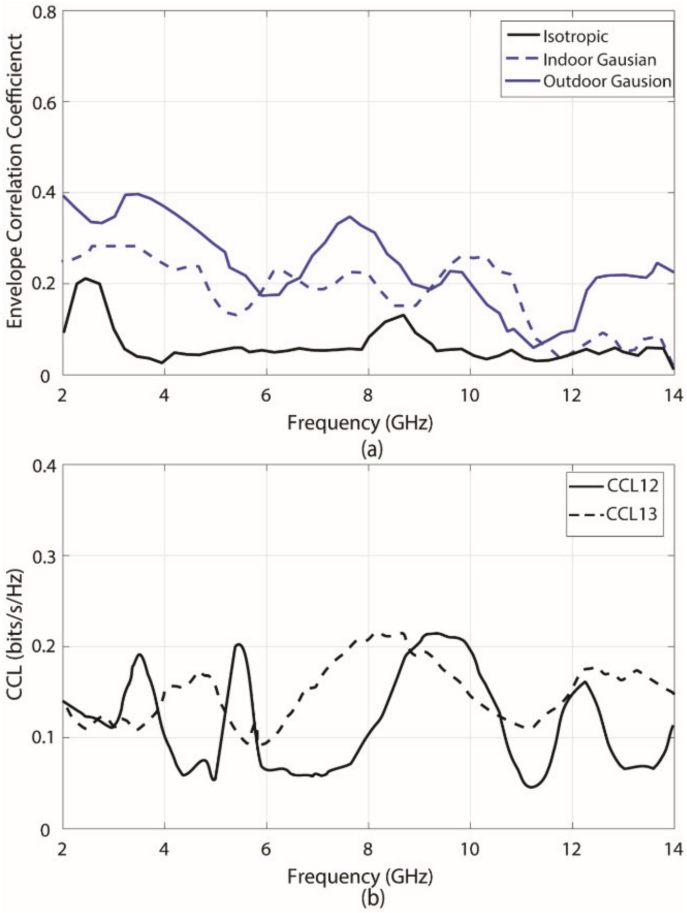

Figure 11. (**a**) Simulated ECC of antenna array computed from far-field radiation patterns for isotropic, indoor and outdoor environments. (**b**) CCL plot over the entire spectrum.

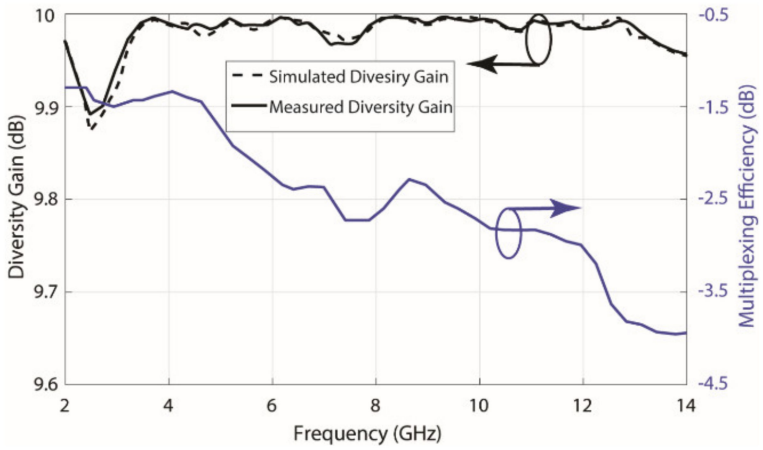

Figure 12. Diversity gain and multiplexing efficiency over the entire spectrum.

The proposed and other recent UWB MIMO antennas are compared in Table 1 to demonstrate the value addition of the proposed work. Although there is a close call between [26] and the proposed work, the proposed design is enhanced in bandwidth by 200 MHz, the mutual coupling is further reduced to −16 dBi from −15 dBi and the efficiency of the design is increased to 90% from 89%. Apparently, the improvement is not particularly significant, but the overall current flow and consequent EM coupling within and across the MIMO antenna, in terms of overall efficiency of the device, matters for the

end user and manufacturers. The deployment of the vertical stubs instead of the square patch used in [26] reduced unwanted interaction between the adjacent radiating patches because of the reduction in overall size of the individual radiating patches, along with an increase in the bandwidth and efficiency of the MIMO antenna. This could also be verified by the decrease in ECC of the proposed antenna to 0.38 from 0.4 and the value of CLL to 0.21 bits/s/Hz from 0.22 bits/s/Hz shown in [26]. Overall, the proposed design is a better candidate in terms of its simplicity to implement, bandwidth, efficiency, mutual coupling, ECC and CLL parameters.

Table 1. The comparison of the proposed UWB MIMO antenna with state-of-the-art antennas.

Reference	Dimension (mm^2)	BW (GHz)	Isolation (dB)	Gain Variation (dBi)	ECC Using Far Field	Radiation Efficiency (%)
[8]	47 × 93	3.1–10.6	<−20	3.5	-	>70
[9]	48 × 34	3.5–10.08	<−23	2.8	<0.039	>75
[10]	80 × 50	4.18–6.58	−17	4	0.056	>80
[11]	40 × 40	3–11	<−17	< 2	-	>75
[12]	50 × 35	1.9–20	<−22	-	0.003	>93
[13]	64 × 45	3.3–7.9	-	3	<0.02	-
[18]	40 × 37.5	2–11	<−20	-	0.1	-
[17]	45 × 45	2–10.6	<−17	4	<0.8	-
[19]	45 × 45	2.2–6.28	<−14	3	<0.25	>65
[20]	40 × 40	3.1–11	<−20	3	<0.004	-
[21]	40 × 40	3–12	<−17	2.9	<0.06	-
[26]	40 × 40	3–13.5	<−15	3.5	<0.4	>89
proposed	40 × 40	2.9–13.6	<−16	3.5	<0.38	>90

4. Conclusions

A printed MIMO antenna is presented here that operates at a broad band of 10.7 GHz ranging from 2.9 to 13.6 GHz, including the FCC-designated UWB (3.1–10.6 GHz). The proposed miniaturized antenna constitutes four stub-loaded circular patch components that are located orthogonally in close proximity to achieve polarization diversity and, thus, improved isolation and reduced size (40 × 40 × 1.524 mm^3). For the entire operating band, i.e., 2.9–13.6 GHz, mutual coupling between different antenna elements is less than −16 dB, and the reflection coefficient is less than −10 dB. The other parameters used to measure and quantify the functionality of a MIMO antenna are also examined, and it is shown that the efficiency of the antenna is greater than 90%, peak gain variations are less than 3.5 dBi, the outdoor Gaussian ECC value is less than 0.38, CCL is less than 0.21 bits/s/Hz, diversity gain is greater than 9.95 dB and multiplexing efficiency is greater than −3.5 dB for the entire frequency range, which validates the functionality of the proposed MIMO antenna. Finally, the proposed printed UWB MIMO antenna is compared to the state-of-the-art MIMO antennas in terms of different parameters, demonstrating that the proposed antenna is a good fit for portable wireless electronic applications in heterogeneous environments.

Author Contributions: Conceptualization, A.A.K., M.S.K., S.A.N., B.I., M.A. (Muhammad Asif), E.M.A. and M.A. (Mohammad Alibakhshikenari); methodology, A.A.K., M.S.K., S.A.N., B.I., M.A. (Muhammad Asif) and M.A. (Mohammad Alibakhshikenari); software, A.A.K., M.S.K., S.A.N. and B.I.; validation, A.A.K., M.S.K., S.A.N., B.I., M.A. (Muhammad Asif), E.M.A., S.K., A.L., M.A. (Mohammad Alibakhshikenari) and E.L.; formal analysis, A.A.K., M.S.K., S.A.N., B.I., M.A. (Muhammad Asif), E.M.A., S.K., A.L., M.A. (Mohammad Alibakhshikenari) and E.L.; investigation, A.A.K., M.S.K., S.A.N., B.I., M.A. (Muhammad Asif), E.M.A., M.A. (Mohammad Alibakhshikenari) and E.L.; resources, A.A.K., M.S.K., S.A.N., B.I., M.A. (Muhammad Asif), M.A. (Mohammad Alibakhshikenari)

and E.L.; data curation, A.A.K., M.S.K., S.A.N., B.I., M.A. (Muhammad Asif), E.M.A., S.K., A.L., M.A. (Mohammad Alibakhshikenari) and E.L.; writing—original draft preparation, A.A.K., and M.S.K.; writing—review and editing, A.A.K., M.S.K., S.A.N., B.I., M.A. (Muhammad Asif), E.M.A., S.K., A.L., M.A. (Mohammad Alibakhshikenari) and E.L.; visualization, A.A.K., M.S.K., S.A.N., B.I., M.A. (Muhammad Asif), M.A. (Mohammad Alibakhshikenari) and E.L.; supervision, M.S.K., S.A.N., B.I., M.A. (Muhammad Asif), M.A. (Mohammad Alibakhshikenari) and E.L.; project administration, M.A. (Mohammad Alibakhshikenari) and E.L.; funding acquisition, S.K., M.A. (Mohammad Alibakhshikenari) and E.L. All authors have read and agreed to the published version of the manuscript.

Funding: This project received funding from Universidad Carlos III de Madrid and the European Union's Horizon 2020 research and innovation program under the Marie Sklodowska-Curie Grant 801538. Furthermore, this work was partially supported by the Researchers Supporting Project number (RSP-2021/58), King Saud University, Riyadh, Saudi Arabia.

Institutional Review Board Statement: Not applicable.

Informed Consent Statement: Not applicable.

Data Availability Statement: All data that support the findings of this study are included within the article.

Acknowledgments: The authors sincerely appreciate the financial support from the Universidad Carlos III de Madrid and the European Union's Horizon 2020 research and innovation program under the Marie Sklodowska-Curie Grant 801538. Moreover, the partial support by the Researchers Supporting Project number (RSP-2021/58), King Saud University, Riyadh, Saudi Arabia, is appreciated.

Conflicts of Interest: The authors declare no conflict of interest.

References

1. Federal Communications Commission. *First Report and Order on Ultra-Wideband Technology*; FCC: Washington, DC, USA, 2002.
2. Alibakhshikenari, M.; Virdee, B.S.; Azpilicueta, L.; Naser-Moghadasi, M.; Akinsolu, M.O.; See, C.H.; Liu, B.; Abd-Alhameed, R.A.; Falcone, F.; Huynen, I.; et al. A Comprehensive Survey of "Metamaterial Transmission-Line Based Antennas: Design, Challenges, and Applications. *IEEE Access* **2020**, *8*, 144778–144808. [CrossRef]
3. Alibakhshikenari, M.; Babaeian, F.; Virdee, B.S.; Aissa, S.; Azpilicueta, L.; See, C.H.; Althuwayb, A.A.; Huynen, I.; Abd-Alhameed, R.A.; Falcone, F.; et al. A Comprehensive Survey on "Various Decoupling Mechanisms with Focus on Metamaterial and Metasurface Principles Applicable to SAR and MIMO Antenna Systems". *IEEE Access* **2020**, *8*, 192965–193004. [CrossRef]
4. Kaiser, T.; Zheng, F.; Dimitrov, E. An Overview of Ultra-Wide-Band Systems with MIMO. *Proc. IEEE* **2009**, *97*, 285–312. [CrossRef]
5. Zhang, Y.H.; Spiegel, R.J.; Fan, Y.; Joines, W.T.; Liu, Q.H.; Xu, K.-D. Design of a Stub-Loaded Ring-Resonator Slot for Antenna Applications. *IEEE Trans. Antennas Propag.* **2015**, *63*, 517–524. [CrossRef]
6. Xu, K.-D.; Luyen, H.; Behdad, N. A Decoupling and Matching Network Design for Single- and Dual-Band Two-Element Antenna Arrays. *IEEE Trans. Microw. Theory Tech.* **2020**, *68*, 3986–3999. [CrossRef]
7. Jiang, C.; Cimini, L.J. Antenna Selection for Energy-Efficient MIMO Transmission. *IEEE Wirel. Commun. Lett.* **2012**, *1*, 577–580. [CrossRef]
8. Radhi, A.H.; Nilavalan, R.; Wang, Y.; Al-Raweshidy, H.S.; Eltokhy, A.A.; Ab Aziz, N. Mutual coupling reduction with a wideband planar decoupling structure for UWB–MIMO antennas. *Int. J. Microw. Wirel. Technol.* **2018**, *10*, 1143–1154. [CrossRef]
9. Tiwari, R.N.; Singh, P.; Kanaujia, B.; Srivastava, K. Neutralization technique based two and four port high isolation MIMO antennas for UWB communication. *AEU-Int. J. Electron. Commun.* **2019**, *110*, 152828. [CrossRef]
10. Jehangir, S.S.; Sharawi, M.S. A Miniaturized UWB Biplanar Yagi-Like MIMO Antenna System. *IEEE Antennas Wirel. Propag. Lett.* **2017**, *16*, 2320–2323. [CrossRef]
11. Mao, C.-X.; Chu, Q.-X. Compact Coradiator UWB-MIMO Antenna with Dual Polarization. *IEEE Trans. Antennas Propag.* **2014**, *62*, 4474–4480. [CrossRef]
12. Chithradevi, R.; Sreeja, B. A compat UWB MIMO antenna with high isolation and low correlation for wireless applications. In Proceedings of the 2017 IEEE International Conference on Antenna Innovations & Modern Technologies for Ground, Aircraft and Satellite Applications (iAIM), Bangalore, India, 24–26 November 2017; IEEE: Piscataway, NJ, USA, 2017; pp. 1–4.
13. Jaglan, N.; Gupta, S.D.; Thakur, E.; Kumar, D.; Kanaujia, B.K.; Srivastava, S. Triple band notched mushroom and uniplanar EBG structures based UWB MIMO/Diversity antenna with enhanced wide band isolation. *AEU-Int. J. Electron. Commun.* **2018**, *90*, 36–44. [CrossRef]
14. Khan, M.S.; Iftikhar, A.; Shubair, R.M.; Capobianco, A.-D.; Braaten, B.D.; Anagnostou, D. Eight-Element Compact UWB-MIMO/Diversity Antenna with WLAN Band Rejection for 3G/4G/5G Communications. *IEEE Open J. Antennas Propag.* **2020**, *1*, 196–206. [CrossRef]

15. Khan, M.S.; Iftikhar, A.; Shubair, R.M.; Capobianco, A.-D.; Asif, S.M.; Braaten, B.D.; Anagnostou, D.E. Ultra-Compact Reconfigurable Band Reject UWB MIMO Antenna with Four Radiators. *Electronics* **2020**, *9*, 584. [CrossRef]
16. Khan, M.S.; Rigobello, F.; Ijaz, B.; Autizi, E.; Capobianco, A.D.; Shubair, R.; Khan, S.A. Compact 3-D eight elements UWB-MIMO array. *Microw. Opt. Technol. Lett.* **2018**, *60*, 1967–1971. [CrossRef]
17. Tripathi, S.; Mohan, A.; Yadav, S. A Compact Koch Fractal UWB MIMO Antenna with WLAN Band-Rejection. *IEEE Antennas Wirel. Propag. Lett.* **2015**, *14*, 1565–1568. [CrossRef]
18. Jafri, S.I.; Saleem, R.; Shafique, M.F.; Brown, A.K. Compact reconfigurable multiple-input-multiple-output antenna for ultra wideband applications. *IET Microw. Antennas Propag.* **2016**, *10*, 413–419. [CrossRef]
19. Anitha, R.; Vinesh, P.V.; Prakash, K.C.; Mohanan, P.; Vasudevan, K. A Compact Quad Element Slotted Ground Wideband Antenna for MIMO Applications. *IEEE Trans. Antennas Propag.* **2016**, *64*, 4550–4553. [CrossRef]
20. Ali, W.A.; Ibrahim, A.A. A compact double-sided MIMO antenna with an improved isolation for UWB applications. *AEU-Int. J. Electron. Commun.* **2017**, *82*, 7–13. [CrossRef]
21. Rajkumar, S.; Amala, A.A.; Selvan, K. Isolation improvement of UWB MIMO antenna utilising molecule fractal structure. *Electron. Lett.* **2019**, *55*, 576–579. [CrossRef]
22. Iqbal, A.; Saraereh, O.A.; Ahmad, A.W.; Bashir, S. Mutual coupling reduction using F-shaped stubs in UWB-MIMO antenna. *IEEE Access* **2017**, *6*, 2755–2759. [CrossRef]
23. Khan, M.S.; Naqvi, S.A.; Iftikhar, A.; Asif, S.M.; Fida, A.; Shubair, R.M. A WLAN band-notched compact four element UWB MIMO antenna. *Int. J. RF Microw. Comput.-Aided Eng.* **2020**, *30*, e22282. [CrossRef]
24. Ray, K.P.; Thakur, S.S. Modified Trident UWB Printed Monopole Antenna. *Wirel. Pers. Commun.* **2019**, *109*, 1689–1697. [CrossRef]
25. Khan, S.M.; Iftikhar, A.; Asif, S.M.; Capobianco, A.-D.; Braaten, B.D. A compact four elements UWB MIMO antenna with on-demand WLAN rejection. *Microw. Opt. Technol. Lett.* **2016**, *58*, 270–276. [CrossRef]
26. Khan, A.A.; Naqvi, S.A.; Khan, M.S.; Ijaz, B. Quad port miniaturized MIMO antenna for UWB 11 GHz and 13 GHz frequency bands. *AEU-Int. J. Electron. Commun.* **2021**, *131*, 153618. [CrossRef]
27. Liu, L.; Cheung, S.W.; Yuk, T.I. Compact MIMO Antenna for Portable Devices in UWB Applications. *IEEE Trans. Antennas Propag.* **2013**, *61*, 4257–4264. [CrossRef]